

Journal of Stress Analysis

Vol. 8, No. 1, 2023-24, 35-55



ORIGINAL RESEARCH PAPER

NSSFEM: Nonlinear Spectral Stochastic Finite Element Method for Analysis of Structures with Elastoplastic Material

Hosseinali Rahimibondarabadi^{*}, Seyed Sajad Mousaviamjad

Department of Civil Engineering, Yazd University, Yazd, Iran.

Article info

Article history:
Received 10 April 2023
Received in revised form
24 August 2023
Accepted 17 September 2023

Keywords:

Karhunen-Loève expansion Polynomial chaos Elastoplastic materials Spectral stochastic finite element method

Abstract

The stochastic finite element method is one of the most effective tools for analyzing systems with uncertainty in computational stochastic mechanics. In this research, a novel approach called the nonlinear spectral stochastic finite element method (NSSFEM) was developed to analyze structures with nonlinear materials. The proposed NSSFEM incorporates uncertainty in both loads and elastic modulus. In the first step, the input random variables are modeled using the operators of NSSFEM, and an appropriate number of terms from the Karhunen-Loève expansion is selected. Next, the stiffness matrix is formed, assuming linear material behavior as the problem-solving begins. Subsequently, the responses are modeled as random processes and expanded using polynomial chaos. During each increment of the solution process, the stress state at the Gaussian points is checked before completing a sub-increment. If the material yielding criteria are activated, the stresses are modified according to plasticity conditions, thereby correcting the solutions. This iterative process continues until the problem is fully resolved and the desired solution is achieved. The displacements obtained through the proposed NSSFEM demonstrate an impressive accuracy of 97% when compared with results from the Monte Carlo method. The source code of the proposed NSSFEM is available at https://github.com/seyedsajadmousavi/NSSFEM

Nomenclature

Ω	Sample space	σ	Algebra in subsets Ω
P	Probability measurements	X	A random variable
$f_x(x)$	Probability density function (PDF)	$\mu_{f(x)}$	Mean of the random field
$\sigma_{f(x)}$	Standard deviation	λ_n	Eigenvalues
$\phi_n(x)$	Eigenfunctions	$C(x_1,x_2)$	Covariance
$k_0^{(e)}$	mean stiffness	$C^{ep}(x,\theta)$	The elastoplastic hardness matrix
$V^{(e)}$	Volume of the element	E	Modulus of elasticity of the materials
$d\sigma(x,\theta)$	Stress increment	$d\epsilon^e(x,\theta)$	Strain increment
$\Delta k^{(e)}$	Stochastic parts of the stochastic stiff-		
	ness matrix		

^{*}Corresponding author: H. Rahimibondarabadi (Associate Professor)

E-mail address: h_rahimi@yazd.ac.ir doi 10.22084/JRSTAN.2024.29190.1255

ISSN: 2588-2597



1. Introduction

1.1. Stochastic Approach in Analysis of Structures

Considering the realization of the scientific community on the importance of the stochastic approach in engineering problems and the significant effect of uncertainties on the behavior of systems, powerful computational methods have been developed. These approaches allow the analysis and design of a variety of engineering systems on a large scale with the help of powerful computing tools considering complex conditions including the application of uncertainty. In structural engineering, uncertainties can include structural inputs such as material properties, geometry, boundary conditions, or loading [1–6]. As the case may be, these properties are described by statistical concepts such as random variables, random processes, or random fields. One of the most useful tools for analyzing systems with uncertainties in computational stochastic mechanics is the stochastic finite element method (SFEM), which is based on the increment of the classical finite element method (FEM). From a mathematical point of view, SFEM can be considered a computational method for solving stochastic partial differential equations [7–12].

1.2. Related Works

In several studies, the problems of convergence and error estimation of this method have been studied in detail. In fact, these two aspects of SFEM are complementary and interdependent. A fundamental problem in stochastic finite element modeling is the uncertainty of system input parameters. The key point of a problem-solving method is the stochastic finite element matrix formulation, which is divided into four general categories based on the calculated technique for modeling uncertainty: Monte Carlo simulation (MCS), perturbation method, spectral decomposition method, and weighted integral method. To obtain system responses, several different SFEMs have been proposed, including the Newman expansion, the Taylorturbulence series expansion method, the stochastic response validation method, the Monte Carlo simulation, and the spectral stochastic finite element method (SSFEM) [13–16]. Due to its capacity to represent a broad range of complicated situations, the Monte Carlo simulation technique is a commonly used simulation approach [13]. The fundamental concept is to construct samples based on the statistical features of random variables, then solve differential equations with stochastic partial derivatives using the finite element technique to obtain a wide variety of solutions. Although relatively accurate results can be obtained by considering the appropriate number of samples, this method is computationally expensive in the problems with a large number of uncertain parameters as well

as large systems. On the other hand, in systems in which the materials used have nonlinear behavior, it is possible to achieve the solution by incremental methods, which itself requires a lot of computational costs. Therefore, in these cases, finding methods that reduce the computational volume will be inevitable [13]. Huo et al. introduced a novel non-intrusive SFEM (NIS-FEM) for usefully calculating stochastic responses and reliabilities of structures. In the first step, the direct probability integral approach (DPIM) was extended to get the PDF of stochastic response by solution of probability density integral equation (PDIE). Then, the NISFEM using DPIM decoupled the classical FEM and PDIE to compute the stochastic output and reliabilities of uncertain plates, and the discretization and quantification of random fields of Young's modulus and thickness were applied via Karhunen-Loève expansion (KLE). The performance of the NISFEM compared with Monte Carlo simulation (MCS) shows that Huo et al. achieved the better accuracy [17]. Andres and Hori proposed a novel method for non-linear elastoplastic bodies based on SFEM, as a generalization of the SFEM for linear elastic materials. The principle characteristic feature of this method was the proposal of two fictitious structures whose behaviors gave maximum and minimum bounds for the mean of variables. The bounding structures are thoroughly derived from a given material feature. The performance of methods is evaluated by MCS. It is illustrated that this method can estimate means and standard divisions of field variables even when the structure has a larger standard division of the body features [18]. Stavroulakis et al. reported the benefits of the graphical processing unit (GPU) for addressing intrusive stochastic mechanics problems. The computational performance of using GPU for solving the problems illustrated an improvement of SSFEM [19].

Sepahvand and Marburg proposed a non-samplingbased SFEM for vibroacoustic analysis of fiberreinforced composite plates with uncertain Young's modulus and damping ratio. The performance evaluation shows numerous effects of uncertainties in diverse frequency ranges. The computed random transmission loss illustrates an acceptable error rate compared to the results obtained by MCS [20]. Appalanaidu et al. introduced a method based on the generalization of stochastic finite element for damage evaluation. The SSFEM is extended where the non-Gaussian random fields are defined by employing an optimal linear expansion scheme. MCS is used to evaluate the stress. The performance of this method is shown with a numerical example including a circular pipe [21]. Researchers have always sought appropriate solutions to this problem, one of which is SSFEM first proposed by Ghanem and Spanos [22]. In this method, KLE is used to discretize a random field that describes uncertain parameters. While the system's responses remain stochastic and are estimated by a chaotic polynomial [13, 20, 23–25]. Since SSFEM has good accuracy and efficiency, it is very popular among researchers and has been used in many studies. This research has been documented in a report. Some studies have used the aforementioned strategy to investigate the following topics: wave propagation analysis, vibration analysis of fiberreinforced composites [20], composite plates [26–28], random creep failure prediction [21], earth dams [29], shells [10, 30], wooden structures [31], elastodynamic issues in the time domain [7], and a variety of other instances have all been investigated. Lacour et al. looked into the nonlinear behavior of uncertain materials without taking into account the loading system's uncertainty, and their findings were provided [32]. However, certain loading was assumed in a wide range from studies presented for SSFEM, the research by Yazdani et al. can be mentioned among the limited researches in which loading is also assumed to be uncertain [13].

The following are the limitations of the state-of-theart:

- Computational complexity to calculate the structural responses
- Speed of accessing the structural responses
- Error rate of the structural responses

1.3. The Proposed Method

In this study, the generalization of SSFEM is utilized to reduce the computational complexity associated with structural responses. The key contributions of this paper are summarized as follows:

- 1) Incorporating uncertainty in materials and loads
- 2) Modeling structures with nonlinear materials
- 3) Reducing computational complexity for calculating structural responses
- 4) Enhancing the speed of accessing structural responses
- 5) Decreasing the error rate of structural responses
- 6) Employing the proposed NSSFEM to analyze the reliability of structures

The remainder of this paper is organized as follows: Section 2 describes the materials and methods. Section 3 introduces the proposed NSSFEM. Results and discussions are presented in Section 4, followed by the conclusion in Section 5.

2. Materials and Methods

The first step in analyzing uncertain systems is to provide system inputs. These inputs usually consist of mechanical and geometric properties as well as system

loading. Some parameters for which uncertainty can be considered include: Young's modulus, Poisson's ratio, yield stress, the cross-sectional geometry of physical systems, material and geometric defects of shells, loading, etc. In general, uncertainty in a complete probability space (Ω, F, P) has been defined, including sample space Ω , algebra σ in subsets Ω , and probability measurements P. In modeling uncertainties in an engineering system, the terms random fields, random processes, and random variables are used when the uncertainties depend on the dimension of space, time, or are independent of both, respectively. An appropriate method to describe these values, which may have uncertainties in time or space is to implement random processes and fields whose probability distributions and correlation structures can be defined through experimental measurements. However, in many cases, there are assumptions about these probabilistic features due to the lack of relevant empirical data. The two main categories of random processes and fields can be defined based on their probability distributions: Gaussian and non-Gaussian. [13, 15, 16, 33–35].

2.1. Random Variables

One way to show uncertainty is to consider the parameters as random variables. Where the variable X, whose value is independent of time and place, is a function for mapping the sample space Ω in a range of real numbers $R(X:\Omega\to R)$. Fig. 1 schematically shows the performance of a random variable.

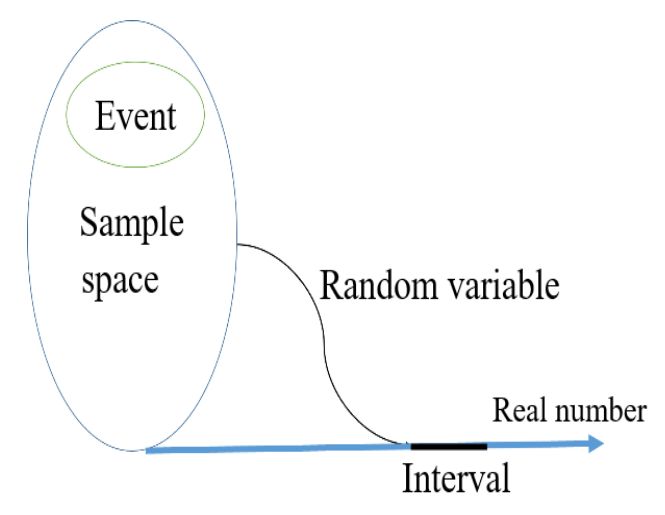


Fig. 1. Schematic performance of a random variable.

The probability of occurrence of a random variable X in the closed interval [a,b] can be calculated by Eq. (1):

$$P(a \le X \le b) = \int_a^b f_x(x) \, \mathrm{d}x \tag{1}$$

Where $f_x(x)$ is a probability density function (PDF).

2.2. Random Field

To address uncertainty in systems, the inputs must first be computed as a random field using a mathematical model capable of expressing a large number of phenomena oscillating in the form of a variable or continuous variables with an unexpected pattern of behavior. If the inputs are treated as a random field, a system of equations with stochastic partial derivatives will dominate, with uncertain and stochastic solutions. KLE and chaotic polynomial expansion (PCE) methods, which are described below, are used to model the random input parameters and system random solutions, respectively.

2.3. Discretization of Random Gaussian Input Fields Using KLE

Despite the fact that most random values in engineering systems are non-Gaussian, the assumption of a possible Gaussian distribution is often used because of the simplicity and lack of relevant experimental data. A wide range of methods developed to simulate Gaussian random processes and fields were used in this study using the KLE method. KLE can be considered as a special case of orthogonal series expansion in which orthogonal functions are selected as special functions of the second type of Fredholm integral Eq. and auto covariance function as the kernel [2, 13, 20, 22, 36, 37]. Suppose that $f(x, \theta)$ represents a random field in the DR domain with a function defined as $(f: D \times \Omega \to R)$ in a perfect probability space (Ω, \mathcal{F}, P) for $x \in D$ and $\theta \in \Omega$ where the mean values of $f(x, \theta)$ are:

$$\mu_{f(x)} = \int_{a}^{b} f(x, \theta) \, \mathrm{d}\theta \tag{2}$$

And for the covariance function $x_1, x_2 \in D$ we will have:

$$C(x_1, x_2) = \langle f(x_1, \theta) - \mu_f(x_1) \rangle \langle f(x_2, \theta) - \mu_f(x_2) \rangle \quad (3)$$

Now if $\mu_{f(x)}$ and $\sigma_{f(x)}$ represent the mean and standard deviation of the random field, respectively, the expansion of KLE will be:

$$f(x,\theta) = \mu_{f(x)} + \sigma_{f(x)} \sum_{n=1}^{N} \sqrt{\lambda_n} \phi_n(x) \xi_n(\theta)$$
 (4)

Where $\mu_{f(x)}$ denotes the mean of the field, λ_n and $\phi_n(x)$ represent the eigenvalues and eigenfunctions of covariance $C(x_1, x_2)$, respectively, n is a set of non-correlated variables, and N represents the number of KLE expansion terms. Also, $\xi_n(\theta)$ is a set of non-correlated random variables with zero mean and unit variance. The eigenvalues and eigenvectors are obtained using the Fredholm quadratic integral equation

as follows:

$$\int_{D} C(x_1, x_2) \phi_n(x_1) \, \mathrm{d}_{x_1} = \lambda_n \phi_n(x_2) \tag{5}$$

2.4. Representation of the Solutions By PCE

Random processes and fields are represented by polynomial chaos (PC), which are created by expanding a series of orthogonal polynomials via a sequence of random variables with definite coefficients [13, 15, 16, 23, 38]. Norbert Wiener presented the PC notion based on the homogeneous PC theory for Gaussian random variables as follows:

$$U(\theta) = a_0 \Gamma_0$$

$$+ \sum_{i_1=1}^{\infty} a_{i_1} \Gamma_1(\xi_{i_1}(\theta))$$

$$+ \sum_{i_1=1}^{\infty} \sum_{i_2=1}^{i_1} a_{i_1 i_2} \Gamma_2(\xi_{i_1}(\theta), \xi_{i_2}(\theta))$$

$$+ \sum_{i_1=1}^{\infty} \sum_{i_2=1}^{i_1} \sum_{i_3=1}^{i_2} a \Gamma_3(\xi_{i_1}(\theta), \xi_{i_2}(\theta), \xi_{i_3}(\theta))$$

$$+ \dots$$
(6)

Where, $a_0, a_{i_1}, a_{i_1 i_2}, \ldots$ are the constant coefficients, and Γ_P is the p-th PC degree of the standard Gaussian random variable obtained as follows:

$$\Gamma_P(\xi) = (-1)^P \frac{\partial^P}{\partial \xi_{i_1} \dots \partial \xi_{i_P}} e^{-\frac{1}{2}\xi^T \xi}$$
 (7)

Now if we want to rewrite Eq. (6) as follows, there is:

$$U(\theta) = u_0 \psi_0(\xi(\theta)) + u_1 \psi_1(\xi(\theta)) + u_2 \psi_2(\xi(\theta)) + \dots$$

$$= \sum_{i=0}^{\infty} u_i \psi_i(\xi(\theta))$$
(8)

Where u_j and ψ_j correspond to $a_0, a_{i_1}, a_{i_1 i_2}, \ldots$ and Γ_P , respectively. Given that the PCE is orthogonal, it meets the following conditions:

$$\psi_0(\theta) = 1, \langle \psi_j(\theta) \rangle = 0, \langle \psi_j(\theta) \psi_k(\theta) \rangle = \langle \psi_j^2(\theta) \rangle \delta_{jk}$$

where δ_{jk} is the kronecker delta.

3. Formulation of a SFEM

The expanded random field is used to formulate the stochastic matrix of each finite element (e). For a special case where the modulus of elasticity is defined as a random spatial variable in a homogeneous random field f(x, y, z), we will have an element to calculate

the stiffness of the element: [13–16]

$$\int_{V^{(e)}} B^{(e)T} D_0^{(e)} B^{(e)} dV^{(e)}
+ \int_{V^{(e)}} B^{(e)T} D_0^{(e)} B^{(e)} f^{(e)}(x, y, z) dV^{(e)}
k^{(e)} = k_0^{(e)} + \Delta k^{(e)}$$
(9)

Where $k_0^{(e)}$ and $\Delta k^{(e)}$ are the mean stiffness and stochastic parts of the stochastic stiffness matrix, respectively. $B^{(e)}$ represents the strain-displacement matrix, $D_0^{(e)}$ is the mean value of the stress-strain matrix, and $V^{(e)}$ denotes the volume of the element. The general stochastic matrix is formed as follows:

$$K = \sum_{i=1}^{Ne} k^e = K_0 + \Delta K \tag{10}$$

Where Ne is the number of finite elements in the problem. Finally, the analysis of stochastic finite elements is obtained by algebraically solving the following equation:

$$P = (K_0 + \Delta K)u \tag{11}$$

Where P and u are node loading and displacement vectors, respectively. Assuming that the modulus of elasticity of the materials (E) used is a Gaussian spatial random variable with a mean of $\mu_E(x)$ and standard deviation of $\sigma_E(x)$, using KLE, it can be represented

$$E(x,\theta) = \mu_{E(x)} + \sigma_{E(x)} \sum_{i=1}^{\infty} \sqrt{\lambda_i} \phi_i(x) \xi_i(\theta)$$
 (12)

$$\begin{bmatrix} K_{00} & K_{01} & & & K_{0,P-2} & K_{0,P-1} \\ K_{10} & K_{11} & & & K_{1,P-2} & K_{1,P-1} \\ & \vdots & & \ddots & & \vdots \\ K_{P-2,0} & K_{P-2,1} & & K_{P-2,P-2} & K_{P-2,P-1} \\ K_{P-1,0} & K_{P-1,1} & & & K_{P-1,P-2} & K_{P-1,P-1} \end{bmatrix} \begin{bmatrix} U_0 \\ U_1 \\ \vdots \\ U_{P-2} \\ U_{P-1} \end{bmatrix} = \begin{bmatrix} F_0 \\ F_1 \\ \vdots \\ F_{P-2} \\ F_{P-1} \end{bmatrix}$$

4. Numerical implementation of incre- or the general strain increment, $d\epsilon(x,\theta)$ as follows: mental elastoplastic relationships

Based on the history of plastic deformations, the incremental solution is derived from the connection between a tiny stress increment and a little strain increment corresponding to the stress state.[39-43] In this part, first, the mechanics of the dissolving process is defined before rewriting the incremental relationships for an elastoplastic material in the form of a matrix. In the matrix form, the stress increment $d\sigma(x,\theta)$ can be expressed by the elastic strain increment term $d\epsilon^e(x,\theta)$ The stochastic stiffness matrix of a finite element is

$$k_i^{(e)}(\theta) = k_0^{(e)} + \sum_{i=1}^{\infty} k_i^{(e)} \xi_i(\theta)$$
 (13)

In the above formulas, the symbols have already been defined.

$$k_i^{(e)} = \sqrt{\lambda_i} \int_{\Omega} \phi_i(x) B^T D_0 B \, \mathrm{d}\Omega \tag{14}$$

Assuming that the load is certain, the equilibrium equation of the finite elements will be as follows:

$$\left[k_0^{(e)} + \sum_{i=1}^{\infty} k_i^{(e)} \xi_i(\theta)\right] U(\theta) = F$$
 (15)

The final equation of equilibrium will be:

$$\left(\sum_{i=0}^{\infty} K_i \xi_i(\theta)\right) \left(\sum_{i=0}^{\infty} U_i \psi_i(\theta)\right) - F = 0$$
 (16)

Finally, a limited number of terms of both expansions are retained. The term M in KLE and the term p in PCE lead to the residue of $\in_{M,P}$, which in the concept of mean squares must be minimized in order to obtain the optimal approximation of the exact solution $U(\theta)$ by polynomial $\psi_i(\theta)$:

$$E[\in_{M,P}\psi_k]=0, k=0,1,2..., P-1$$
 (17)

After several algebraic operations in a system with N degrees of freedom with $P = \frac{(M+p)!}{M!p!}$, the linear system of equations with dimensions $(N \times P) * (N \times P)$

$$\begin{bmatrix} U_0 \\ U_1 \\ \vdots \\ U_{P-2} \\ U_{P-1} \end{bmatrix} = \begin{bmatrix} F_0 \\ F_1 \\ \vdots \\ F_{P-2} \\ F_{P-1} \end{bmatrix}$$
 (18)

$$\{d\sigma(x,\theta)\} = [C(x,\theta)]\{d\epsilon^{e}(x,\theta)\}$$

$$= [C(x,\theta)](\{d\epsilon(x,\theta)\} - \{d\epsilon^{P}(x,\theta)\}) \quad (19)$$

$$\{d\sigma(x,\theta)\} = [C^{ep}(x,\theta)]\{d\epsilon(x,\theta)\} \quad (20)$$

The increment of plastic strain $\{d\epsilon^P(x,\theta)\}$ is expressed using a dependent rule as follows:

$$\{ d\epsilon^P(x,\theta) \} = d\lambda \frac{\partial f}{\partial \{\sigma(x,\theta)\}}$$
 (21)

Where $\frac{\partial f}{\partial \{\sigma(x,\theta)\}}$ is a gradient vector of the yield

function $f(\sigma_{ij}(x,\theta); k(x,\theta))$. The scalar function $d\lambda$ is expressed as Eq. (22):

$$\mathrm{d}\lambda = \frac{L}{h} \tag{22}$$

Where L is the function of the loading criterion defined in Eq. (23):

$$L = \left\{ \frac{\partial f}{\partial \{\sigma(x,\theta)\}} \right\}^T [C(x,\theta)] \{ d\epsilon(x,\theta) \}$$
 (23)

The scalar function h is defined in Eq. (24):

$$h = \left\{ \frac{\partial f}{\partial \{\sigma(x,\theta)\}} \right\}^{T} [C(x,\theta)] \left\{ \frac{\partial f}{\partial \{\sigma(x,\theta)\}} \right\} + A^{'} \quad (24)$$

Where A' is:

$$A' = -\frac{dk(x,\theta)}{d\in} C \sqrt{\left\{\frac{\partial f}{\partial \{\sigma(x,\theta)\}}\right\}^T \left\{\frac{\partial f}{\partial \{\sigma(x,\theta)\}}\right\}}$$

$$\frac{\partial f}{\partial k(x,\theta)} \tag{25}$$

Where:

$$k(x,\theta) = \frac{\sigma_{yv}(x,\theta) + E_p(x,\theta)(\epsilon(x,\theta) - \epsilon^e(x,\theta))}{\sqrt{3}}$$

$$\to \frac{\mathrm{d}k(x,\theta)}{d\epsilon}$$

$$= \frac{E_p(x,\theta)}{\sqrt{3}}$$
(26-a)

$$C = \sqrt{\frac{2}{3}} \tag{26-b}$$

$$\frac{\partial f}{\partial k(x,\theta)} = -2k(x,\theta) = -\frac{2}{\sqrt{3}}\sigma_{yv}(x,\theta) \tag{26-c}$$

And for a material with a hardening model, we will have bilinear:

$$E_p(x,\theta) = \frac{E(x,\theta)E_T(x,\theta)}{E(x,\theta) - E_T(x,\theta)}$$
(27)

Finally, the elastoplastic hardness matrix $[C^{ep}(x,\theta)]$ is:

$$[C^{ep}(x,\theta)] = [C(x,\theta)] - \frac{[C(x,\theta)] \left\{ \frac{\partial f}{\partial \{\sigma(x,\theta)\}} \right\} \left\{ \frac{\partial f}{\partial \{\sigma(x,\theta)\}} \right\}^T [C(x,\theta)]}{\left\{ \frac{\partial f}{\partial \{\sigma(x,\theta)\}} \right\}^T [C(x,\theta)] \left\{ \frac{\partial f}{\partial \{\sigma(x,\theta)\}} \right\} + A'}$$
(28)

For the plane stress state, when the von Mises yield criterion is used, $\left\{\frac{\partial f}{\partial \{\sigma(x,\theta)\}}\right\}$ is obtained as follows:

$$\left\{ \frac{\partial f}{\partial \{\sigma(x,\theta)\}} \right\} = \left\{ \begin{array}{c} \frac{2\sigma_{11}(x,\theta) - \sigma_{22}(x,\theta)}{3} \\ \frac{2\sigma_{22}(x,\theta) - \sigma_{11}(x,\theta)}{3} \\ 2\sigma_{12}(x,\theta) \end{array} \right\}$$
(29)

Stress calculations will be performed for all Gaussian points. In the following, the calculations will be considered for only one Gaussian point. In step (m+1), the stresses ${}^m\{(x,\theta)\sigma\}$ and the strains ${}^m\{\epsilon(x,\theta)\}$ in step m are specified, and the hardening parameters $({}^mk(x,\theta)$ and ${}^m{}_p(x,\theta))$ are also calculated at the end of the step m. For a typical iteration step, i-th approximate displacement ${}^{m+1}\{U\}^{(i)}$ is obtained from the (m+1)-th increment of the load. The strain and strain increment corresponding to this displacement at the Gaussian point will be as follows:

$$^{m+1}\{\epsilon\}^{(i)} = [B]^{m+1}\{U\}^{(i)}$$
 (30)

$$\{\Delta\epsilon(x,\theta)\} = {}^{m+1}\{(x,\theta)\epsilon\}^{(i)} - {}^m\{\epsilon(x,\theta)\}$$
 (31)

First, assuming that the behavior of materials during the strain increment calculated in Eq. (31) remains in the elastic range, the elastic stress increment equivalent to this strain increment is calculated as follows:

$$\{\Delta \sigma^e(x,\theta)\} = [C(x,\theta)] \{\Delta \epsilon(x,\theta)\}$$
 (32)

Assuming that at the end of the m-th increment, the stress state at the Gaussian point satisfies the elastic state conditions $f(^m\{\sigma(x,\theta)\}; ^mk(x,\theta)) < 0$ and in the increment (m+1) enters an elastoplastic state $f(^m\{\sigma\} + \{\Delta\sigma^e\}; ^mk) > 0$. Therefore, there is a scaling factor (Fig. 2) "r" for which it will be: $f(^m\{\sigma(x,\theta)\} + r\{\Delta\sigma^e(x,\theta)\}; ^mk(x,\theta)) = 0$. Then, the strain will be divided into two parts $r\{\Delta\epsilon(x,\theta)\}$ and $(1-r)\{\Delta\epsilon(x,\theta)\}$. The first part deals with the fully elastic response of materials, while the second part is related to the response of elastoplastic materials. Therefore, the stress increment can be obtained from the following integral as follows:

$$\{\Delta\sigma(x,\theta)\} = \int_{m_{\{\epsilon(x,\theta)\}}}^{m+1_{\{\epsilon(x,\theta)\}}} [C(x,\theta)](\{d\epsilon(x,\theta)\})$$

$$-\{d\epsilon^{P}(x,\theta)\})$$

$$= \int_{m_{\{\epsilon(x,\theta)\}}}^{m_{\{(\kappa,\theta)\epsilon\}+r_{\{\Delta\epsilon(x,\theta)\}}}} [C(x,\theta)]\{d\epsilon(x,\theta)\}$$

$$+ \int_{m_{\{\epsilon(x,\theta)\}+r_{\{\Delta\epsilon(x,\theta)\}}}}^{m_{\{\epsilon(x,\theta)\}+r_{\{\Delta\epsilon(x,\theta)\}}}} [C(x,\theta)]$$

$$-\{d\epsilon^{P}(x,\theta)\}$$

$$-\{d\epsilon^{P}(x,\theta)\}$$

$$-\{d\epsilon^{P}(x,\theta)\}$$

$$-\{d\epsilon^{P}(x,\theta)\}$$

$$+ \int_{m_{\{\epsilon(x,\theta)\}+r_{\{\Delta\epsilon(x,\theta)\}}}}^{m_{\{\epsilon(x,\theta)\}+r_{\{\Delta\epsilon(x,\theta)\}}}} [C(x,\theta)]$$

$$-\{d\epsilon(x,\theta)\}-\{d\epsilon^{P}(x,\theta)\}$$

$$-\{d\epsilon^{P}(x,\theta)\}$$

Finally, the stress corresponding to $^{m+1}\{U\}^{(i)}$ will 4.2. Calculation of the scale factor "r" be obtained as follows:

$$^{m+1} \{ \sigma(x,\theta) \}^{(i)} = ^{m} \{ \sigma(x,\theta) \} + \{ \Delta \sigma(x,\theta) \}$$
 (35)

4.1. Determination of the loading state

The first step in stress calculations is to determine the loading state of a Gaussian point; in other words, to determine whether the Gaussian point is in the state corresponding to the strain increment $(\{\Delta \epsilon(x,\theta)\})$ in the plastic loading state, the elastic state, or in the loading state. Only in situations when the plastic load is dominating, the elastoplastic relations are applied. The governing ties are more flexible in other circumstances. The state of materials is analyzed in two entirely different scenarios for this aim. The first state corresponds to the Gaussian point being in an elastic state at the conclusion of step m, whereas the second state relates to the Gaussian point being in an elastoplastic state. If the end point of the m-th Gaussian point is in the elastic state, $f(^m\{\sigma(x,\theta)\}; ^mk(x,\theta)) < 0$, assuming that it is created by applying the strain increment, the state of the Gaussian point remains in the elastic state, and the corresponding stress increment is calculated using Eq. (32). According to the stress obtained based on the above hypothesis, the state of the Gaussian point is examined. If the yield criterion confirms the correctness of the initial hypothesis that the position of the Gaussian point is in the elastic state, $f(^m \{\sigma(x,\theta)\} + \{\Delta \sigma^e(x,\theta)\}; ^m k(x,\theta)) < 0$ at the end of increment (m + 1), all stress calculations at the Gaussian point can be calculated based on elasticity relations. However, if the study of the yield criterion indicates that the materials yield, $f(^{m}\{\sigma(x,\theta)\} + \{\Delta\sigma^{e}(x,\theta)\}; ^{m}k(x,\theta)) > 0$, the calculation of scale factor "r" of the fully elastic strain must be separated from the elastoplastic strain. Then, the stress increment in the elastic part is calculated using the calculated elasticity relations, and the governing elastoplastic relationships are used for calculating the stress increment in the elastoplastic part.

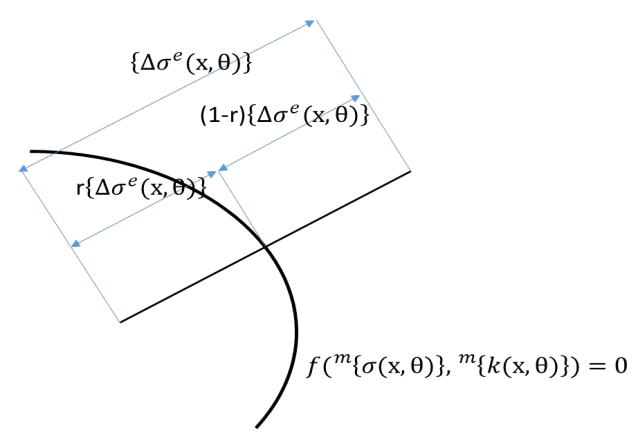


Fig. 2. Schematic representation of the scale factor rto separate the elastic part from the elastoplastic part.

The scale factor "r" is shown schematically in Fig. 2. To obtain the scale factor, Eq. (36) should be solved. Eq. (36) can be solved both analytically and numerically. If the yield equation is expressed simply based on the invariables, the solution can be analytically obtained; otherwise it is necessary to use numerical methods to solve Eq. (36).

$$f(^{m}\lbrace \sigma(x,\theta)\rbrace + r\lbrace \Delta\sigma^{e}(x,\theta)\rbrace; ^{m}k(x,\theta)) = 0$$
 (36)

Due to the simplicity of the equation form, the von Mises criteria may be solved both analytically and numerically. As a result, both analytical and numerical approaches to obtaining the scale factor for the von Mises yield criterion will be described in this section. However, it should be noted that the iterative procedure is used to determine the scale factor of numerical techniques in general. With the isotropic hardening model, the usual equations for the von Mises yield are:

$$f(\{\sigma(x,\theta)\}, k(x,\theta)) = \frac{1}{2} \{S(x,\theta)\}^T \{S(x,\theta)\} - k^2 (\epsilon_P(x,\theta))$$
(37)

Where $\{S(x,\theta)\}\$ is the vector of deviator stresses defined as follows:

$$\{S(x,\theta)\}^T = \{S_x(x,\theta); S_y(x,\theta); S_z(x,\theta); S_{yz}(x,\theta); S_{zx}(x,\theta); S_{xy}(x,\theta)\}$$
(38)

The increment of the deviator stress is also defined as follows:

$$\{\Delta S(x,\theta)\}^{T} = \{\Delta S_{x}(x,\theta), \Delta S_{y}(x,\theta), \Delta S_{z}(x,\theta), \Delta S_{yz}(x,\theta), \Delta S_{zx}(x,\theta), \Delta S_{xy}(x,\theta)\}$$
(39)

To analytically solve Eq. (36) based on deviator stresses and the increment of deviator stresses, we have:

$$f(^{m}\{\sigma(x,\theta)\}+r\{\Delta\sigma^{e}(x,\theta)\},^{m}k(x,\theta))$$

$$=\frac{1}{2}(^{m}\{S(x,\theta)\}+r\{\Delta S(x,\theta)\})^{T}$$

$$(^{m}\{S(x,\theta)\}+r\{\Delta S(x,\theta)\})-^{m}k^{2}(\epsilon_{P}(x,\theta))$$

$$=0$$
(40)

$$\frac{1}{2}r^{2}\{\Delta S(x,\theta)\}^{T}\{\Delta S(x,\theta)\} + r^{m}\{S(x,\theta)\}^{T}\{\Delta S(x,\theta)\} + \frac{1}{2}^{m}\{S(x,\theta)\}^{Tm}\{S(x,\theta)\} - mk^{2}(\epsilon_{P}(x,\theta)) = 0$$
(41)

Hence, the scale factor r is obtained by solving Eq.

$$\frac{1}{2}r^{2}\{\Delta S(x,\theta)\}^{T}\{\Delta S(x,\theta)\} + r^{m}\{S(x,\theta)\}^{T}\{\Delta S(x,\theta)\} + \frac{1}{2}^{m}\{S(x,\theta)\}^{Tm}\{S(x,\theta)\} - mk^{2}(\epsilon_{P}(x,\theta)) = 0 \tag{42}$$

To numerically solve an iterative process until we solution will be presented in Eq. (43). reach the desired error rate, the general process of this

$$r^{(i)} = \frac{f(^{m}\{\sigma(x,\theta)\}, ^{m}k(x,\theta))}{f(^{m}\{\sigma(x,\theta)\}, ^{m}k(x,\theta)) - f(^{m}\{\sigma(x,\theta)\} + \{\Delta\sigma^{e}(x,\theta)\}, ^{m}k(x,\theta))}$$

$$r^{(i+1)} = r^{(i)} - \frac{f(^{m}\{\sigma(x,\theta)\} + r^{(i)}\{\Delta\sigma^{e}(x,\theta)\}, ^{m}k(x,\theta))}{f(^{m}\{\sigma(x,\theta)\} + r^{(i-1)}\{\Delta\sigma^{e}(x,\theta)\}, ^{m}k(x,\theta)) - f(^{m}\{\sigma(x,\theta)\} + r^{(i)}\{\Delta\sigma^{e}(x,\theta)\}, ^{m}k(x,\theta))} (r^{(i-1)} - r^{(i)})$$

$$(43)$$

4.3. Integration Techniques

The algorithms used to integrate Eq. (33) or (34) can be divided into two categories: One group is based on explicit techniques and the other group is based on implicit techniques. For both types, to achieve the required accuracy in the integration process, the elastoplastic strain increment can be divided into an appropriate number of n, which is called sub-increment, $\{\Delta \widetilde{\in} (x,\theta)\}.$

$$\{d\epsilon(x,\theta)\} = \{\Delta \widetilde{\in} (x,\theta)\} = \frac{(1-r)\{\Delta \in (x,\theta)\}}{n}$$
 (44)

Forward stresses are estimated from one strain subincrement to the next, if an explicit procedure is employed, such as the Euler forward method. The stresses at the end of each sub-increment are computed again, if an implicit approach is employed, such as the Euler backward method. Hence, in this case, there are two iterative loops in solving nonlinear equations, one is the iteration loop of equilibrium equations, and the other is during the integration process to evaluate the accuracy of stresses. In this section, we will only discuss some details of the explicit Euler forward method. For each sub-increment, $\{\Delta \widetilde{\in} (x,\theta)\}$, the explicit method includes the following steps:

Step 1: Determine the plastic strain increment using $\{\Delta \tilde{\epsilon}^p\}$ with a suitable algorithm and determine the effective plastic strain increment $\Delta \widetilde{\in}_p$.

$$\{\Delta \widetilde{\epsilon}^p(x,\theta)\} = \frac{(1-r)}{n} \frac{L}{h} \left\{ \frac{\partial f}{\partial \{\sigma(x,\theta)\}} \right\}$$
 (45)

Step 2: Calculate the stress sub-increment $\{\Delta \widetilde{\sigma}(x,\theta)\}\$

$$\{\Delta \widetilde{\sigma}(x,\theta)\} = [C(x,\theta)](\{\Delta \widetilde{\epsilon}(x,\theta)\} - \{\Delta \widetilde{\epsilon}^p(x,\theta)\})$$
(46)

Step 3: Update the stress, strain and hardening parameters:

$$\{\sigma(x,\theta)\} \leftarrow \{\sigma(x,\theta)\} + \{\Delta \widetilde{\sigma}(x,\theta)\}
\{ \in (x,\theta)\} \leftarrow \{\epsilon(x,\theta)\} + \{\Delta \widetilde{\in}(x,\theta)\}
\{ \in^{P}(x,\theta)\} \leftarrow \{ \in^{P}(x,\theta)\} + \{\Delta \widetilde{\epsilon}^{p}(x,\theta)\}
\epsilon_{P}(x,\theta) \leftarrow \epsilon_{P}(x,\theta) + \Delta \widetilde{\in}_{p}(x,\theta), k \leftarrow k(\epsilon_{P}(x,\theta))$$

$$(47)$$

4.4. Modification of the Increments to Satisfy Compatibility Conditions

Compatibility conditions df = 0 must be met in a plastic loading process. However, since many approximations are used in a numerical solution, the compatibility conditions are often not met. Adding a strain sub-increment to the next load state results in:

$$f(\lbrace \sigma(x,\theta)\rbrace;\epsilon_P(x,\theta))\neq 0$$
 (48)

In other words, the stress is not on the next yield surface and moves away from the yield surface. Such a stress deviation accumulates from the vield surface and leads to very important errors for solving nonlinear equations. As a result, the stress vector must be changed to meet the compatibility requirements. Adding a correction vector in the direction of the normal yield surface vector to the stress vector is a common way to do so.

$$\{\delta\sigma(x,\theta)\} = a \left\{ \frac{\partial f}{\partial \{\sigma(x,\theta)\}} \right\}$$

$$a = \frac{-f(\{\sigma(x,\theta)\}, k(x,\theta))}{\left\{ \frac{\partial f}{\partial \{\sigma(x,\theta)\}} \right\}^T \left\{ \frac{\partial f}{\partial \{\sigma(x,\theta)\}} \right\}}$$
(49)

Finally, the modified stress vector will be obtained:

$$\{\sigma(x,\theta)\} \leftarrow \{\sigma(x,\theta)\} + \{\delta\sigma(x,\theta)\} \tag{50}$$

4.5. Formulation of the Structures with Nonlinear Materials in SSFEM:

To use SSFEM for solving uncertain structures with nonlinear materials, first, by using the operators of this method and selecting the appropriate number of terms from KLE and PCEs, the input random variables and solution are modeled. Then, the process of solving the stiffness matrix is formed and assuming that the behavior of the materials is linear, the problem begins to be solved. In each increment, before a solution subincrement is completed, the stress state at the Gaussian points is checked so that if the material yielding criteria are activated, the operators of the plastic condition applications modify the stresses and, consequently, the solutions are corrected. This process continues until the problem is completely solved and the desirable solution is achieved.

4.6. Structural Reliability Analysis Based on Spectral Finite Element Method

In the sense of structural reliability, the probability of failure occurs when the load and material properties are random variables (X), and structural failure can be estimated using a finite state function (g(x)) defined for the structure response. The failure probability is then calculated using the multiple integral defined in the failure domain $Df = \{g(x) \leq 0\}$ as follows [33]:

$$P_f = \operatorname{prob}[g(x) \le 0] = \int_{Df} f(x) \, \mathrm{d}x \tag{51}$$

Where f(x) is PDF x and prob is a measure of probability. Since Eq. (51) is difficult to solve in most engineering problems, various numerical methods were proposed for these problems. Since the output of stochastic spectral finite elements is a structural stochastic response vector, it could be easy to calculate the PDF and CDF of the responses and the probability of structural failure using MCS. The probability of failure can be approximated as follows:

$$P_f = \frac{n}{N} \tag{52}$$

Where n is the number of samples for $g(x) \leq 0$, and Ns is the total number of samples. The reliability index (β) in MCS is defined as follows:

$$\beta = -\Phi^{-1}(P_f) \tag{53}$$

Where Φ is the CDF of normal standard.

5. Numerical Examples

5.1. Example 1: A Square Plate

Fig. 3 shows a plate in the plane stress mode with dimensions of 160 * 160 * 2mm, zero material density and Poisson's coefficient of 0.3 under four concentrated horizontal loads p1 in three nodes, 2,3 and 4 and three concentrated vertical loads p2 in nodes 10,15 and 20 that, the specifications of the loads are listed in Table 1. The support is between rigid nodes 1 to 21. For analysis, loading, modulus of elasticity E (Fig. 4) and yield stress S are considered as random fields with mean and standard deviation σ . All three parameters are defined based on Eq. (54) using the two-dimensional exponential function. bx and by are correlation lengths, which

are assumed to be equal to 160 in both directions, and for a KLE with 4 terms, eigenvalues and eigenvectors are shown in Fig. 5 and Fig. 6. In this case, the maximum acceptable displacement is 6mm. In this example, by changing the number of M and p, the effect of increasing and decreasing the number of KLE terms and the order of PCE on the accuracy of the results are evaluated.

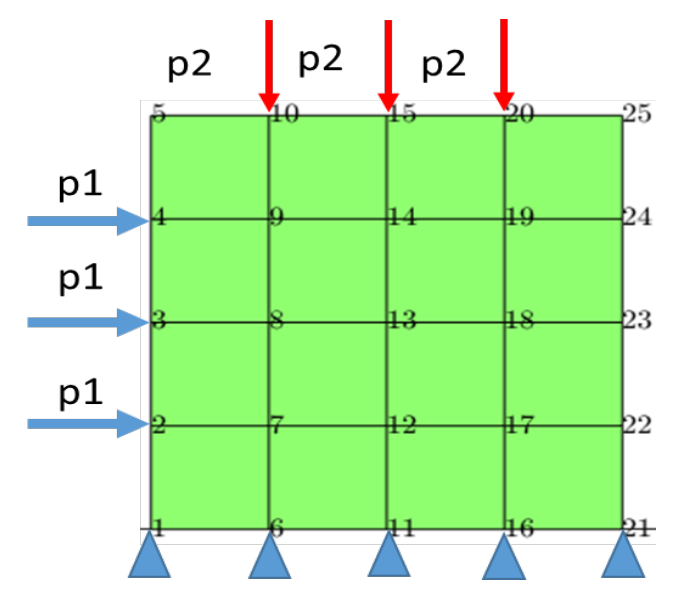


Fig. 3. The structure examined in example 1.

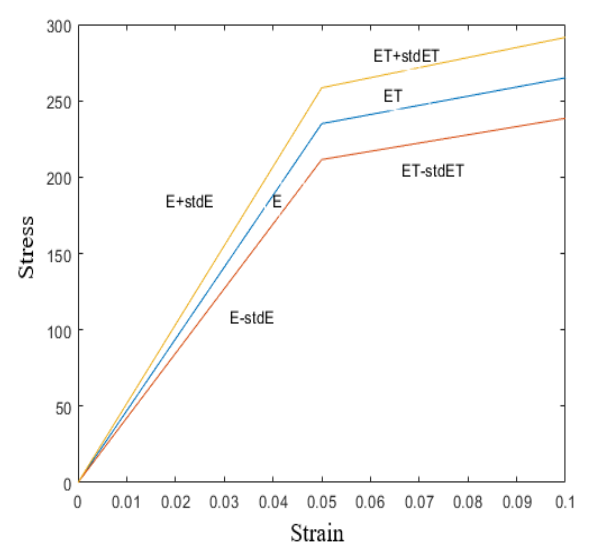


Fig. 4. Modulus of elasticity of the materials in examples 1 and 2.

Table 1
Structure input specifications of example 1.

Value	Parameter	Value	Parameter	Value	Parameter	Value	Parameter
25	Nodes	235MPa	μS	20GPa	$\mu \mathrm{ET}$	20000N	μ p1
16	Elements	23.5MPa	σS	2GPa	$\sigma \mathrm{ET}$	2000N	σ p1
$40 \text{mm} \times 40 \text{mm}$	Mesh size	160	bx	200GPa	$\mu { m E}$	30000N	$\mu \mathrm{p}2$
		160	by	20GPa	$\sigma \mathrm{E}$	3000N	σ p2

$$C(X_1, X_2) = \exp\left(-\frac{|x_1, x_2|}{b_x} - \frac{|y_1, y_2|}{b_y}\right)$$
 (54)

The mean displacements and stresses and standard deviations resulted from NSSFEM can be seen in Fig. ??. By examining the results obtained from the proposed method and comparing these data with the outputs of the Monte Carlo method (10,000 samples were evaluated in both examples), the accuracy of the proposed solution was very favorable due to the reduction of computation time. Figs. 7 and 8 provide a comparison between the PDFs as well as the CDFs obtained for vertical displacement at node 25 and the accuracy

based on different Ms and ps. Based on the results presented in these figures, it can be found that the effect of increasing the M term is more than p in achieving the desirable result. On the other hand, M has an effect on the accuracy of the obtained values, and p has a very effective effect on the scatter of responses. The accuracy of the findings is high, with an error rate of less than 3%. Fig. 9 shows the relationship between the mean displacement values produced using the Monte Carlo approach and NSSFEM. Table 2 shows the results of the NSSFEM and MCS techniques for the chance of failure and computation time.

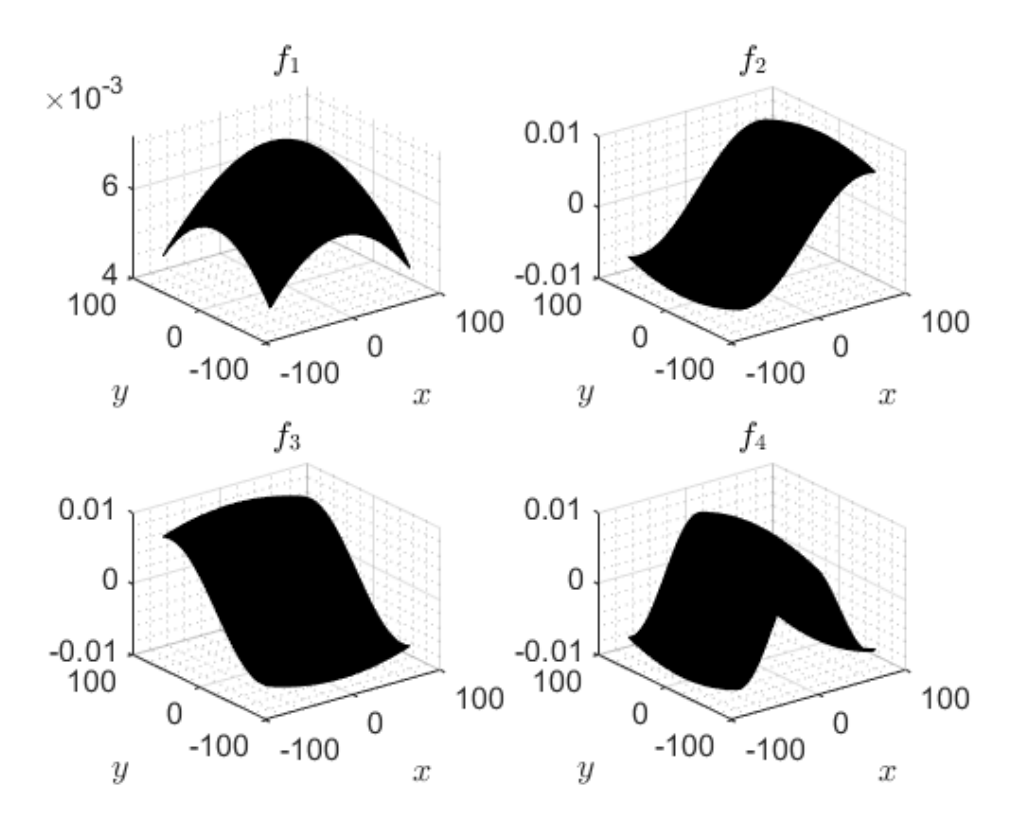


Fig. 5. Eigenvalues for 4 KLE terms in 2 dimensions.

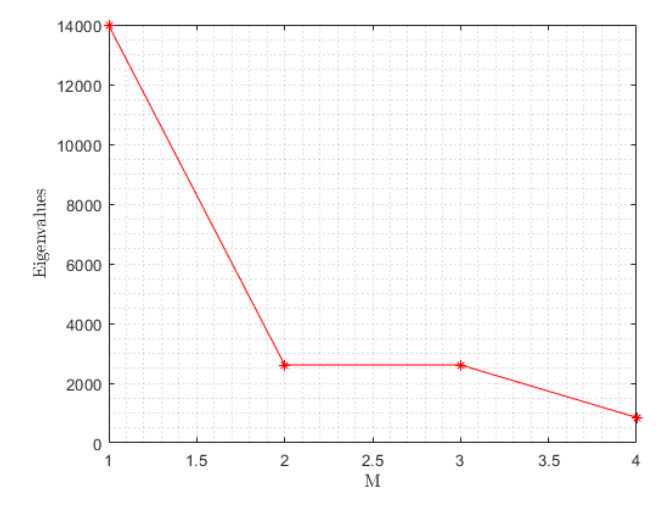


Fig. 6. Eigenvectors for 4 KLE terms in 2 dimensions.

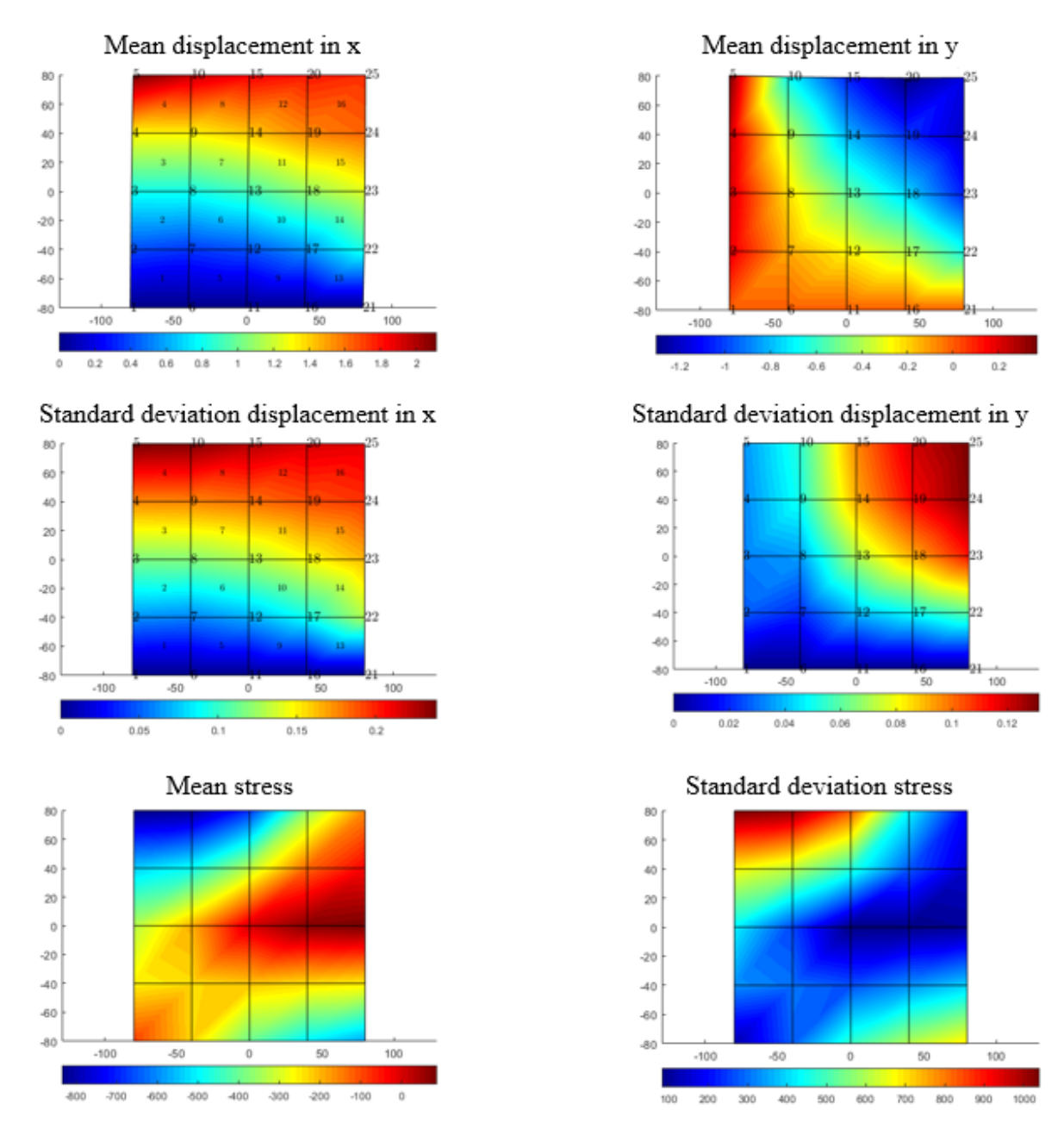


Fig. 7. Mean and standard deviation of displacement and stress in the structure example 1.

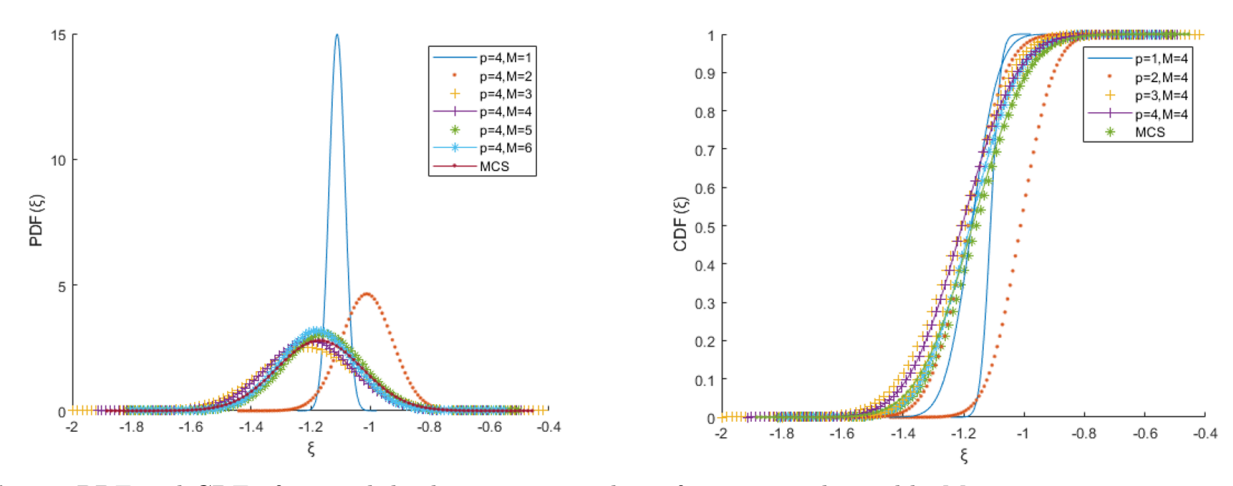
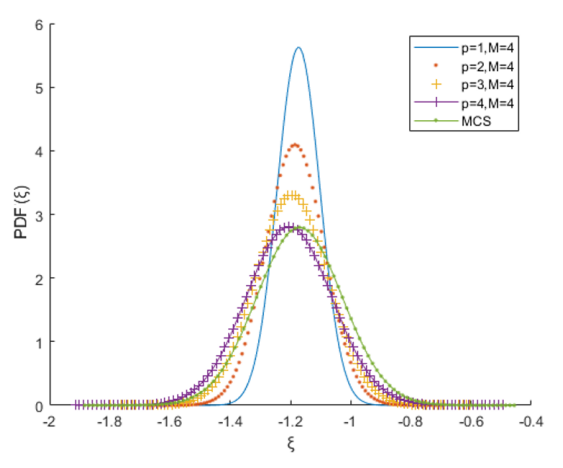


Fig. 8. PDF and CDF of vertical displacement at node 25 for p=4 and variable Ms.



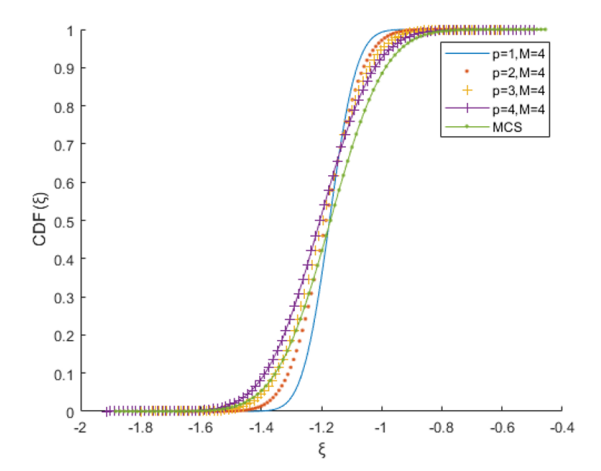


Fig. 9. PDF and CDF of vertical displacement at node 25 for M=4 and variable p.

 ${\bf Table~2} \\ {\bf Probability~of~failure~and~structural~analysis~time~of~example~1}.$

Time (sec)	β	Pf	Case
17362	2.2058	0.0137	MCS
1273	2.2286	0.01292	NSSFEM

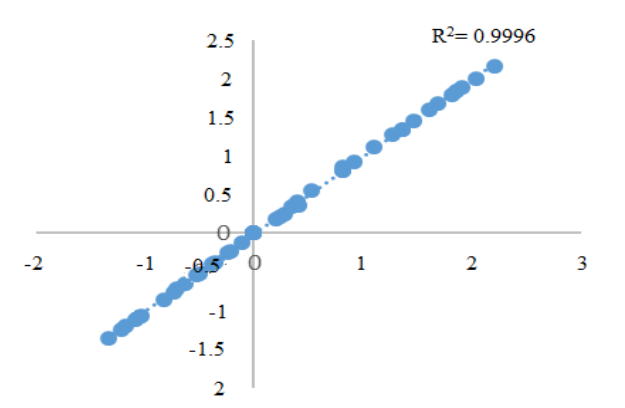


Fig. 10. Correlation between mean displacement values obtained from Monte Carlo method and SSFEM $M=4,\ p=3.$

5.2. Example 2: A square plate with a central cut-out

Fig. 13 shows a square plate with a central cut-out with three different meshings in the plane stress mode with dimensions of 120*120*2mm. The density of materials is assumed to be zero and the Poisson's ratio to be 0.3. Structures under a wide vertical load q, three concentrated horizontal loads p1, and two concentrated vertical loads p2, where the locations of the

loads in each mesh were shown in Table 3, and the load specifications are presented in Table 4. The location of the joint support for each mesh is given in Table 3. For analysis of loading, modulus of elasticity E (Fig. 4) and yield stress S are considered as random fields with a mean and standard deviation σ . All three parameters are defined according to Eq. (54) using the two-dimensional exponential function. bx and by are correlation lengths assumed to be equal to 120 in both directions, and eigenvalues and eigenvectors for a KLE with 4 terms are displayed in Figs. 10 and 11.

In this case, the reliability analysis is performed using type 3 meshing, and a maximum acceptable displacement of 10mm is considered.

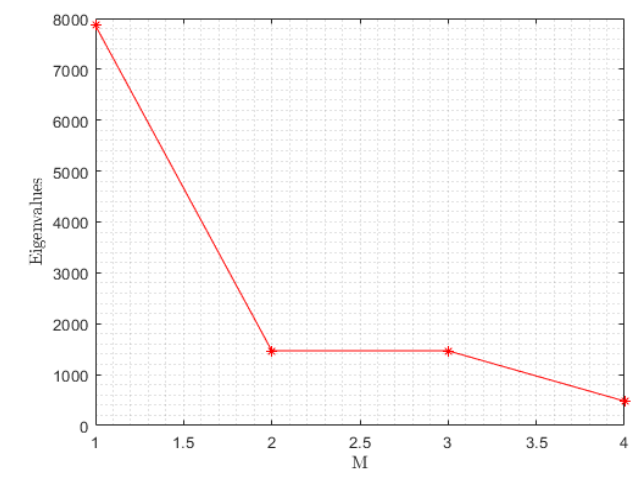


Fig. 11. Eigenvalues for 4 KLE terms in 2 dimensions for example 2.

 ${\bf Table~3} \\ {\bf Meshing~specifications~and~location~of~loads~and~supports~in~each~meshing~in~example~2}.$

		1.1	0 1			
location of loads	location of loads	location of loads	Mesh	Number of	Number of	Mesh
q	p2 (nodes)	p1 (nodes)	size	nodes	elements	
Between nodes4-16	4,16	2, 3,4	$40\text{mm} \times 40\text{mm}$	16	9	Mesh1
Between nodes7-48	7,48	3, 5,7	$20\mathrm{mm}{\times}20\mathrm{mm}$	48	32	Mesh2
Between nodes13-160	13,160	13, 9,5	$10\mathrm{mm}{\times}10\mathrm{mm}$	160	128	Mesh3

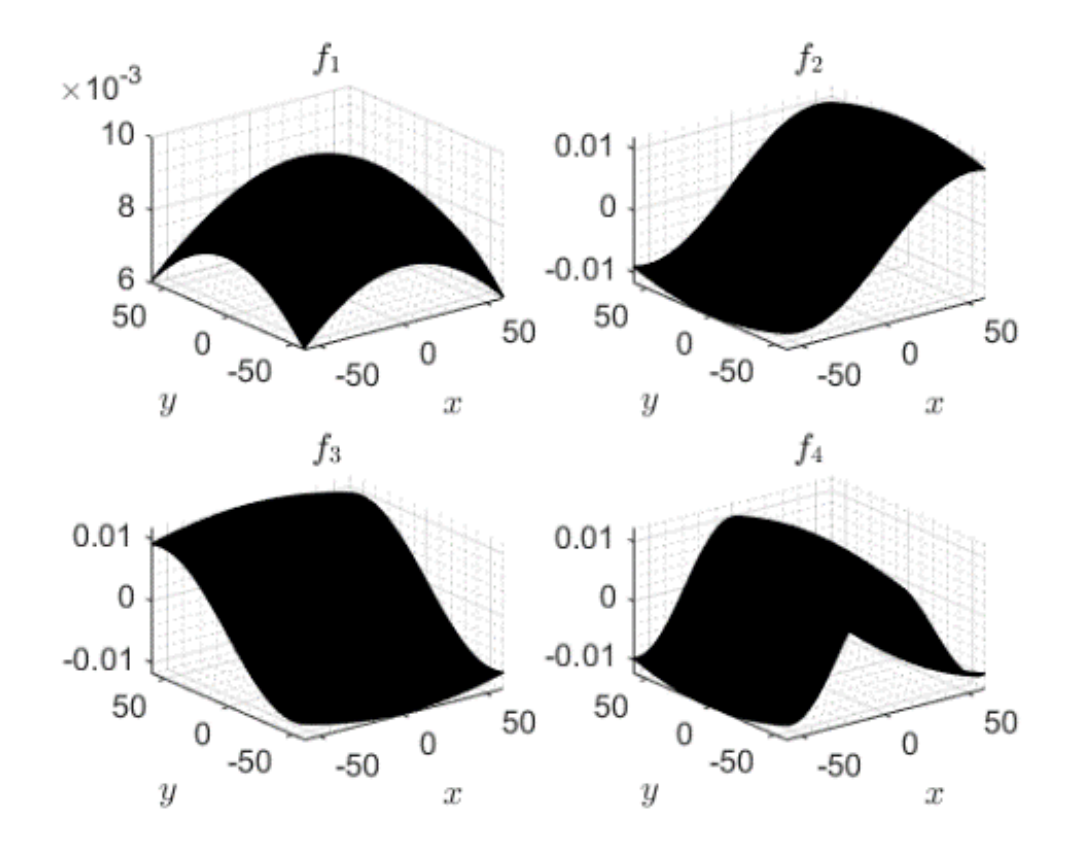


Fig. 12. Eigenvectors for 4 KLE terms in 2 dimensions for example 2.

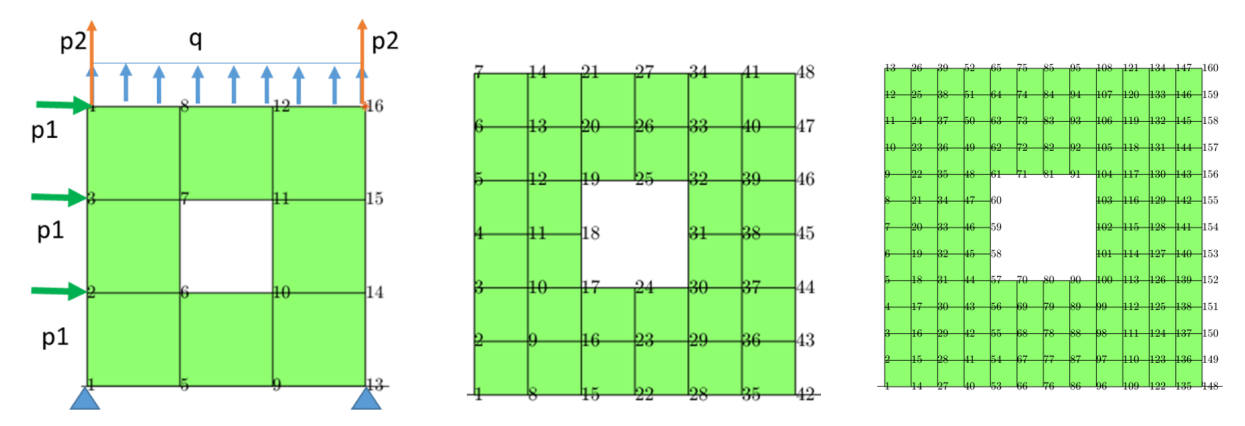


Fig. 13. Structural meshing of example 2.

Table 4
Structural input data of example 2.

Value	Parameter	Value	Parameter	Value	Parameter
100GPa	$\mu \ \mathrm{ET}$	1000N	$\mu p2$	$200\mathrm{N/mm}$	μq
10GPa	$\mathrm{ET}\sigma$	100N	$\sigma p2$	$20\mathrm{N/mm}$	$q\sigma$
235MPa	μ S	200GPa	μE	6~000N	$\mu p1$
23.5MPa	σS	20GPa	$\mathrm{E}\sigma$	600N	$\sigma p1$

Three different sizes of meshing are utilized in this example to demonstrate how to achieve the desired solution and the impact of meshing dimensions. The findings were produced for varying M and p using two

forms of meshing 1 and 2 and compared to the values acquired using the Monte Carlo approach (Figs. 13-20). By viewing the PDF and CDF diagrams (Figs. 13, 14-16, and 18-20) obtained for the displacements, it can

be seen that by increasing the KL and PCE terms, the accuracy of the results is increased to the point that in both meshings with p=4, M=4, the mean value and standard deviation of displacement in the nodes with an error percentage of less than 4% correspond to the values obtained from Monte Carlo (Figs. 16, 20, and 23). For the third meshing, only p=4, M=4 were used in modeling the probabilistic parameters, the results of which can be observed in Figs. 21, 22, and 23. Fig. 23

shows the correlation between the outputs of MCS and NSSFEM, which can clearly show the resultant consistency. In this example, the mean error is less than 4%. Mean displacements and stresses and standard deviations obtained from NSSFEM can be seen in Figs. 13, 17, and 21 for all three types of meshing. The values obtained for the probability of failure as well as the duration of calculations of both NSSFEM and MCS are presented in Table 5.

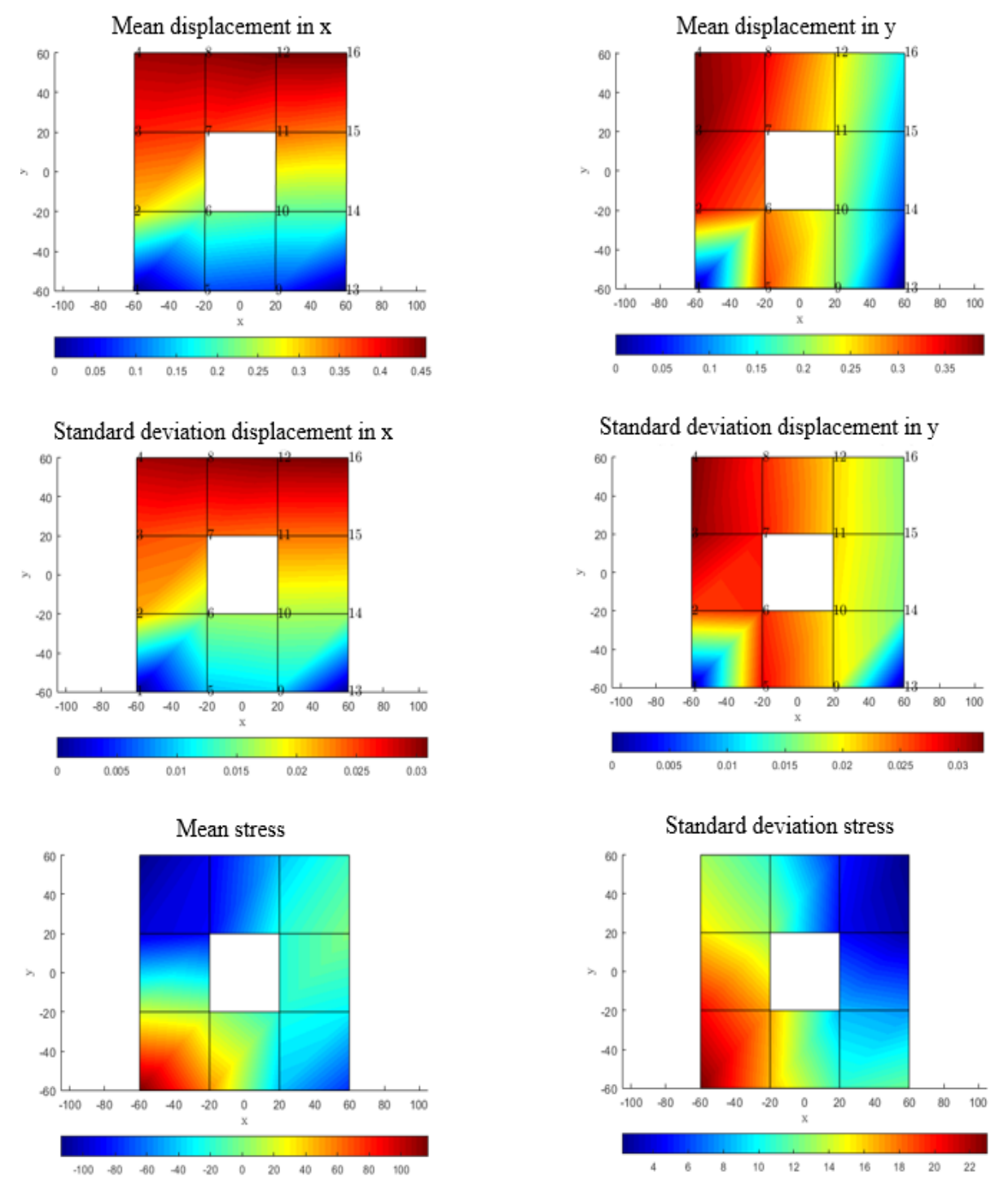


Fig. 14. Mean and standard deviation of displacement and stress in the structure of example 2, meshing No. 1.

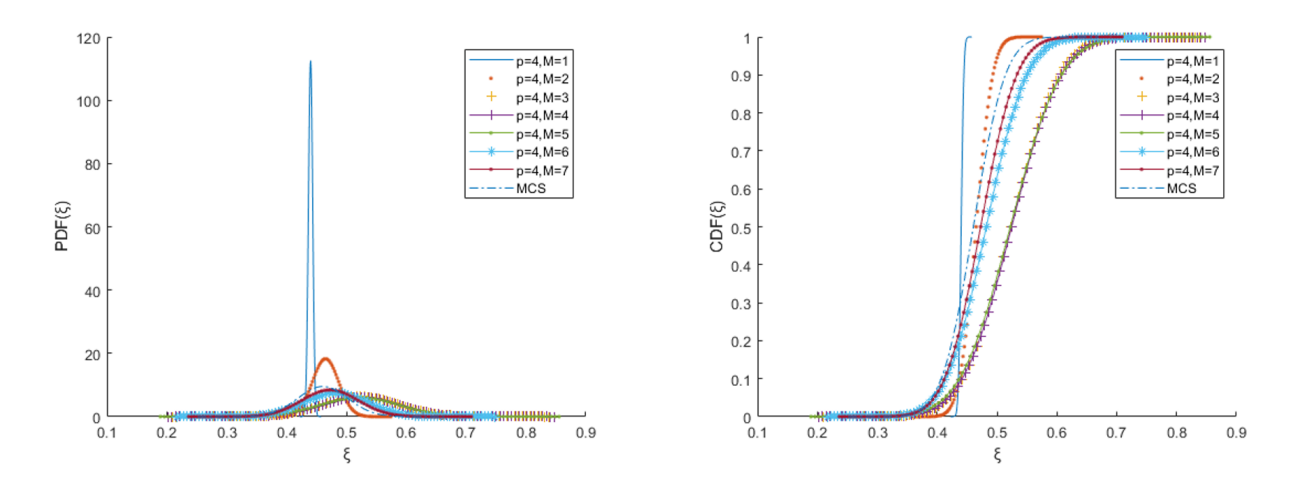


Fig. 15. PDF and CDF of horizontal displacement at node 16 for p=4 and variable Ms.

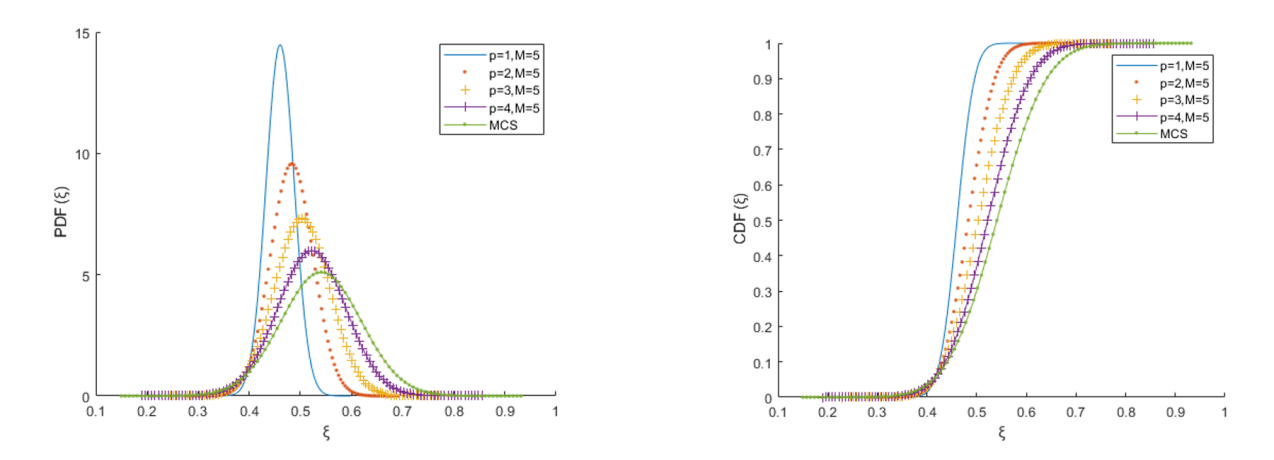


Fig. 16. PDF and CDF of horizontal displacement at node 16 for M=5 and variable p.

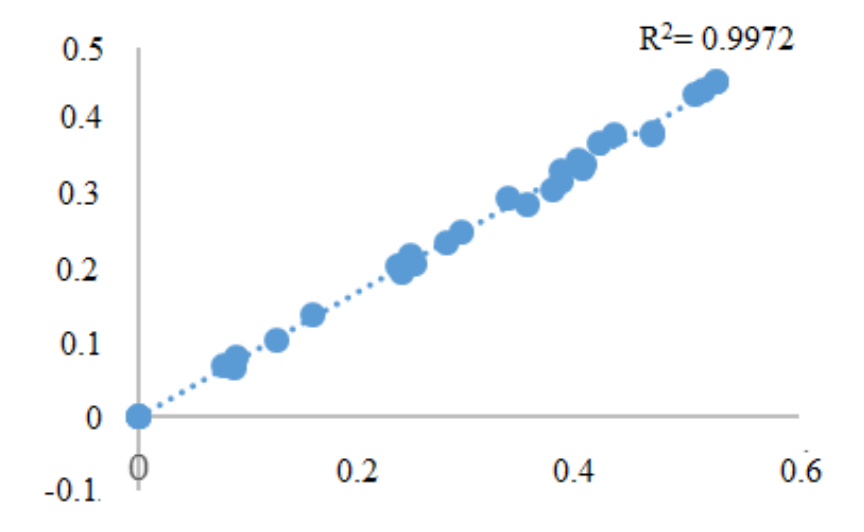


Fig. 17. Correlation between the mean displacement values obtained for meshing 1 of example 2 of the Monte Carlo method and the SSFEM M=4, p=4.

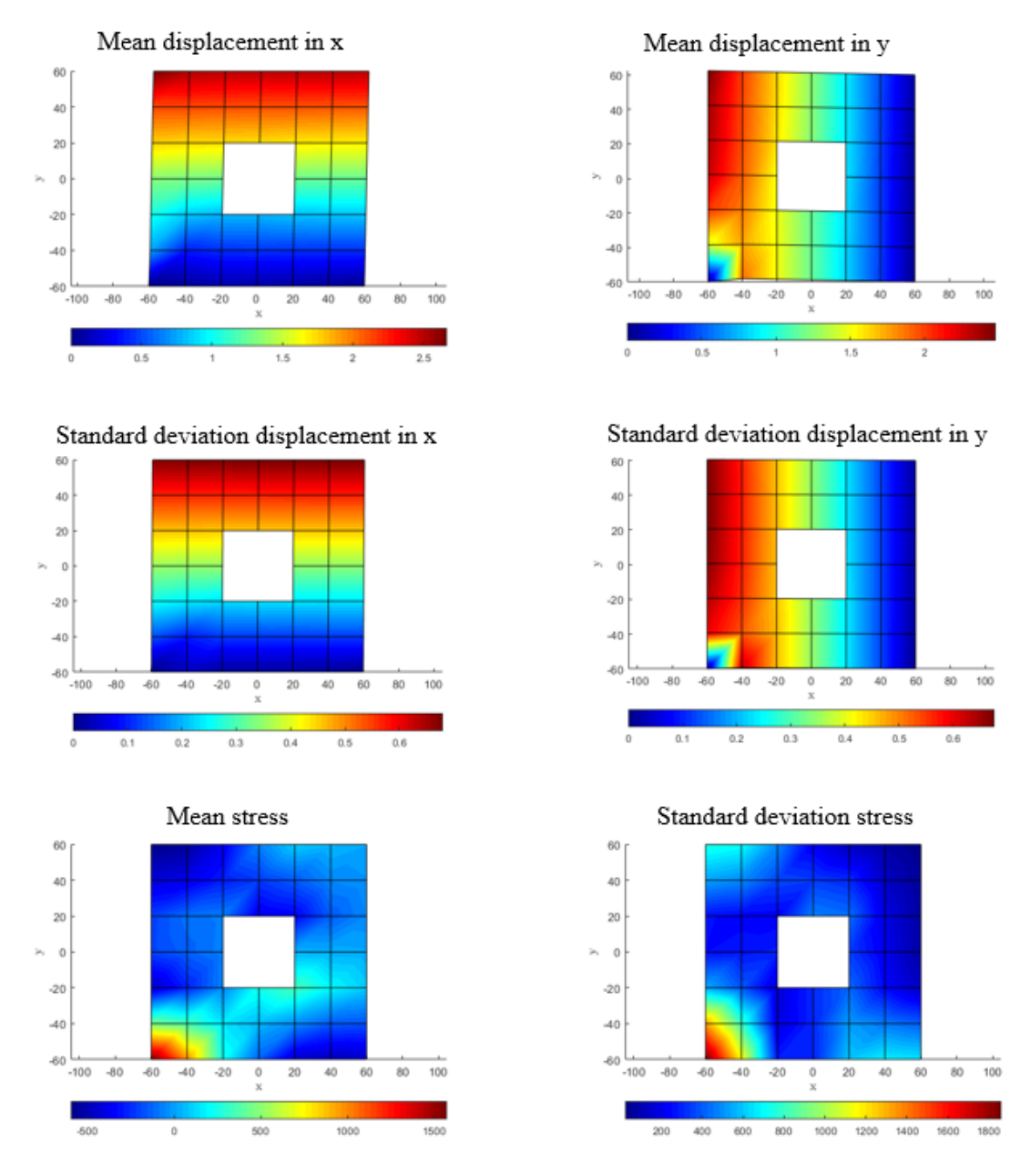
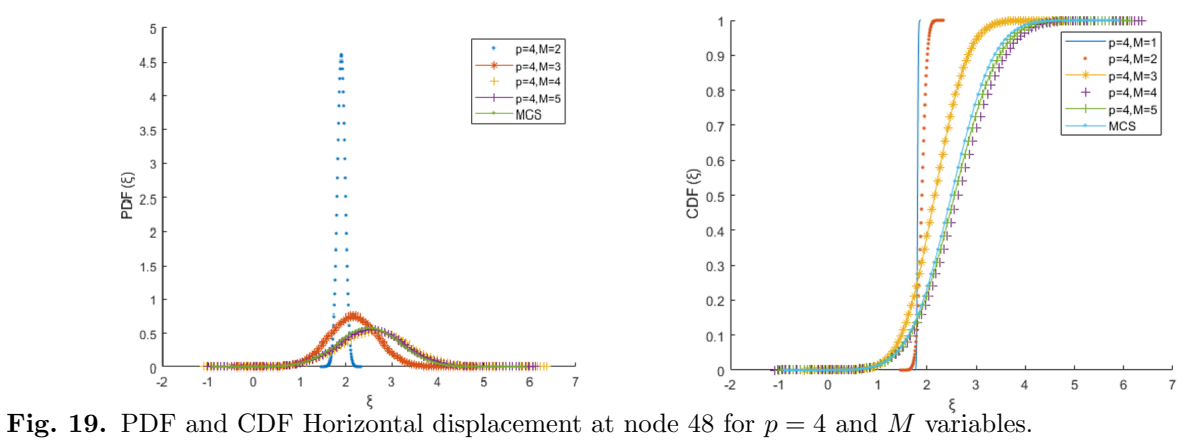


Fig. 18. Mean and standard deviation of displacement and stress in the structure of example 2; Meshing No.



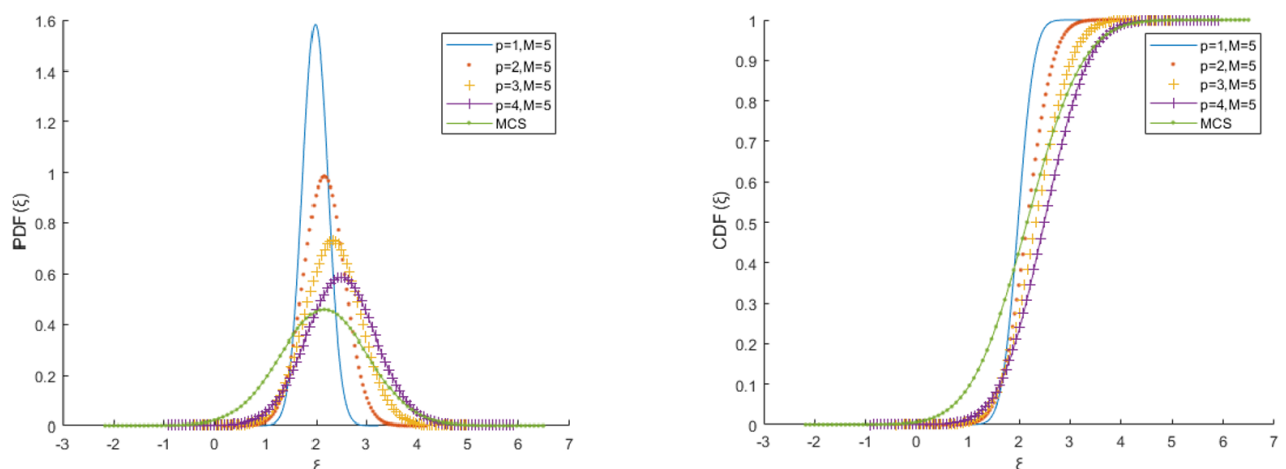


Fig. 20. PDF and CDF of horizontal displacement at node 16 for M=5 and variable p.

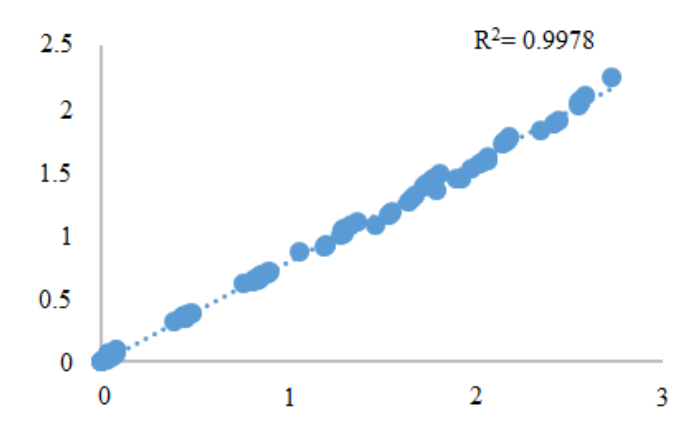


Fig. 21. Correlation between the mean displacement values obtained for meshing 3 of example 2 for the Monte Carlo method and the SSFEM M=4, p=4.

Table 5
Probability of failure and structural analysis time of example 2.

Time (sec)	β	Pf	Case
1375265	3.2835	0.0112	MCS
115421	3.2476	0.0123	NSSFEM

6. Conclusions

Factoring in uncertainty in the structure's input parameters complicates the problem, particularly because nonlinear analysis is both time-consuming and computationally intensive. To address this, we introduced the nonlinear spectral stochastic finite element method (NSSFEM), which generalizes the SSFEM for nonlinear problems. The proposed NSSFEM incorporates uncertainties in both materials and loads, making it applicable to structures modeled with elastoplastic materials. Our modeling results demonstrate that using NSSFEM, as opposed to Monte Carlo Simulation (MCS), significantly reduces the computation time required to obtain structural responses. Additionally,

NSSFEM achieves an error rate of less than 3% in these responses. The proposed NSSFEM was also utilized to analyze the reliability of structures. The values of the Karhunen-Loève expansion (KLE) and polynomial chaos expansion (PCE) terms were optimized. The findings indicate that increasing the number of KLE terms (M) has a greater impact on accuracy than increasing the order of PCE (p). Moreover, both increasing and decreasing KLE terms are more effective in enhancing the result accuracy. This study shows that larger structures require fewer KLE and PCE terms to achieve the desired level of accuracy. Overall, the results from NSSFEM demonstrate 97% accuracy while significantly reducing the computation time.

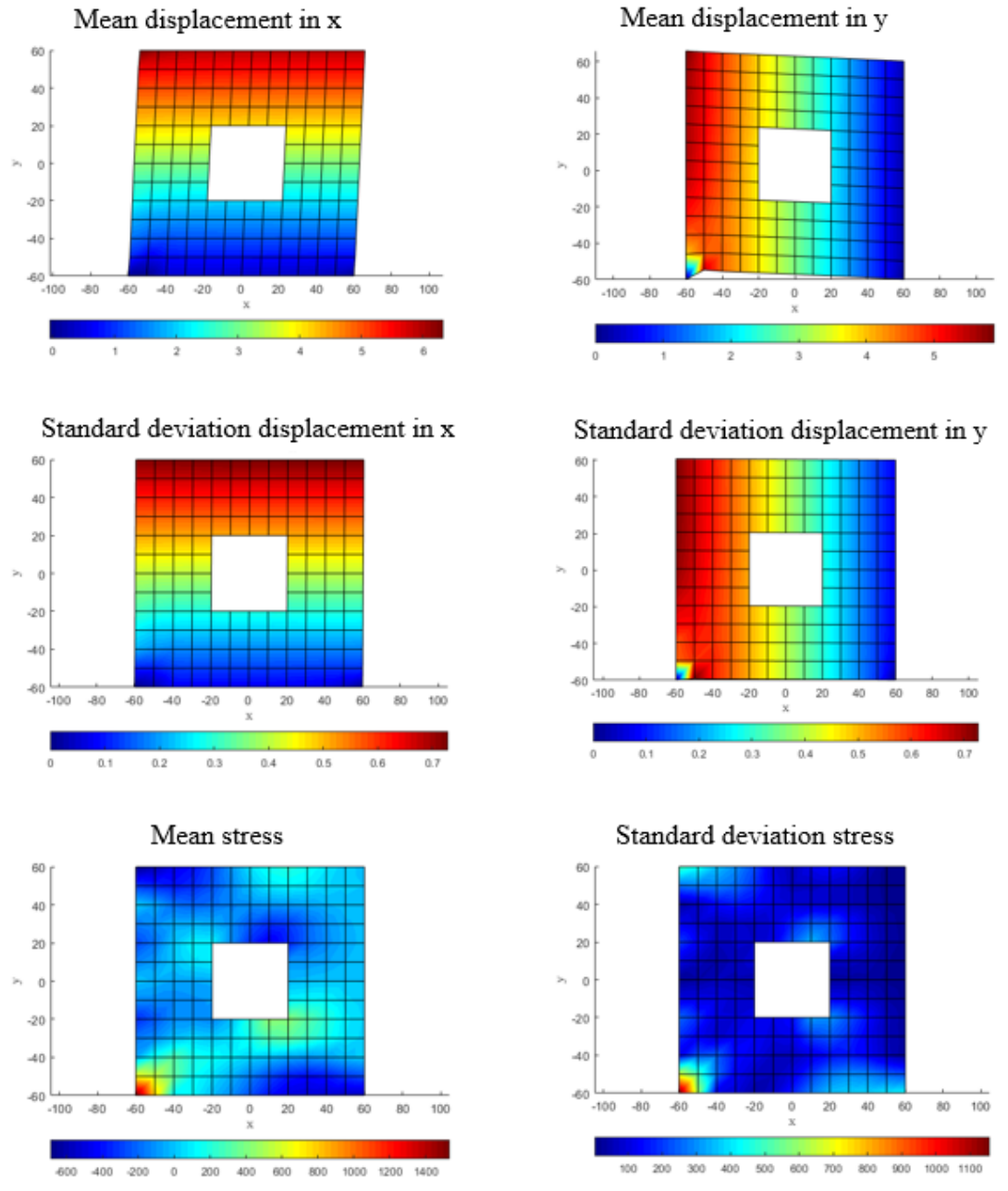


Fig. 22. Mean and standard deviation of displacement and stress in the structure of example 2; meshing No. 3.

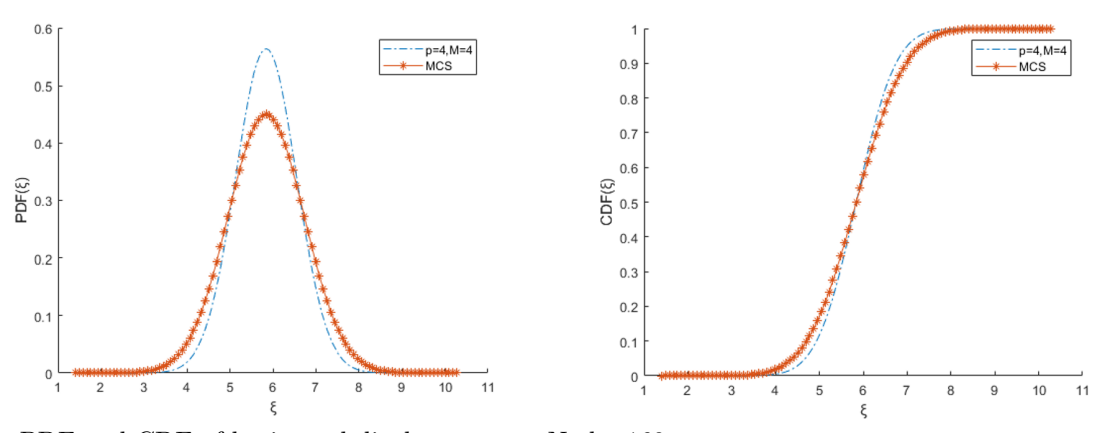


Fig. 23. PDF and CDF of horizontal displacement at Node 160.

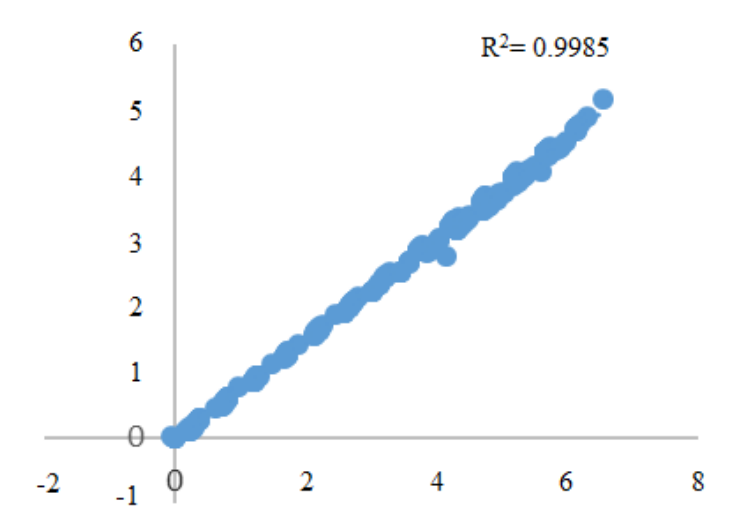


Fig. 24. Correlation between the mean displacement values obtained for meshing 3 of example 2 for the Monte Carlo method and the SSFEM M = 4, p = 4.

References

- Z. Zheng, H. Dai, "Structural stochastic responses determination via a sample-based stochastic finite element method," Comput. Methods Appl. Mech. Eng., vol. 381, (2021), doi: 10.1016/j.cma.2021.113824.
- [2] M.R. Machado, S. Adhikari, J.M.C. Dos Santos, "A spectral approach for damage quantification in stochastic dynamic systems," Mech. Syst. Signal Process., 88 (2017) 253-273, doi: 10.1016/j.ymssp.2016.11.018.
- [3] D.E.M. Bouhjiti, J. Baroth, F. Dufour, S. Michel-Ponnelle, and B. Masson, "Stochastic finite elements analysis of large concrete structures' serviceability under thermo-hydromechanical loads-Case of nuclear containment buildings," Nucl. Eng. Des., 370 (2020), doi: 10.1016/j.nucengdes.2020.110800.
- [4] F. Wu, K. Chen, T.Y. Wang, L.Y. Yao, M. Hu, "Stochastic hybrid perturbation technique-based smoothed finite element-statistical energy method for mid-frequency analysis of structure–acoustic systems with parametric and non-parametric uncertainties," Comput. Methods Appl. Mech. Eng., 349 (2019) 522-549, doi: 10.1016/j.cma.2019.02.034.
- [5] S. Dutta, S. Ghosh, "Form-finding of framesupported tensile membrane structures using stochastic optimisation," Structures, 32 (2021) 2211-2221, doi: 10.1016/j.istruc.2021.03.103.
- [6] S. Shang, G.J. Yun, "Stochastic finite element with material uncertainties: Implementation in a general purpose simulation program,"

- Finite Elem. Anal. Des., 64 (2013) 65-78, doi: 10.1016/j.finel.2012.10.001.
- [7] P. Zakian, N. Khaji, "A novel stochastic-spectral finite element method for analysis of elastodynamic problems in the time domain," Meccanica, 51(4) (2016) 893-920, doi: 10.1007/s11012-015-0242-9.
- [8] F. Bouchoucha, M.N. Ichchou, M. Haddar, "Diffusion matrix through stochastic wave finite element method," Finite Elem. Anal. Des., 64 (2013) 97-107, doi: 10.1016/j.finel.2012.09.008.
- [9] G.E. Zouraris, I. Babuška, R. Tempone, "Galerkin finite element approximations of stochastic elliptic partial differential equations," SIAM J. Numer. Anal., 42(2) (2004) 800-825, [Online]. Available: http://epubs.siam.org/doi/abs/10.1137/S00361 42902418680.
- [10] Y.P. Liang, X. Ren, D.C. Feng, "Efficient stochastic finite element analysis of irregular wall structures with inelastic random field properties over manifold," Comput. Mech., (2021) 1-17, doi: 10.1007/s00466-021-02084-4.
- [11] G. Stefanou, M. Papadrakakis, "Stochastic finite element analysis of shells with combined random material and geometric properties," Comput. Methods Appl. Mech. Eng., vol. 193(1-2) (2004) 139-160, doi: 10.1016/j.cma.2003.10.001.
- [12] M.F. Ngah, A. Young, "Application of the spectral stochastic finite element method for performance prediction of composite structures," Compos. Struct., 78(3) (2007) 447-456, doi: 10.1016/j.compstruct.2005.11.009.

- [13] A. Yazdani, H. Ghohani Arab, M. Rashki, "Simplified spectral stochastic finite element formulations for uncertainty quantification of engineering structures," Structures, 28 (2020) 1924-1945, doi: 10.1016/j.istruc.2020.09.040.
- [14] G. Stefanou, "The stochastic finite element method: Past, present and future," Comput. Methods Appl. Mech. Eng., 198(9-12) (2009) 1031-1051, doi: 10.1016/j.cma.2008.11.007.
- [15] R.G. Ghanem, P.D. Spanos, Stochastic Finite Elements: A Spectral Approach. Courier Dover Publications, (1991). doi: 10.1007/978-1-4612-3094-6.
- [16] D.G.G. Vissarion Papadopoulos, Stochastic Finite Element Methods. Springer, (2018).
- [17] H. Huo, W. Xu, W. Wang, G. Chen. D. Yang, "New non-intrusive stochastic finite element method for plate structures," Comput. Struct., 268 (2022),10.1016/j.compstruc.2022.106812.
- [18] M. Anders, M. Hori, "Stochastic finite element method for elasto-plastic body,"
 Int. J. Numer. Methods Eng., 46 (11) (1999) 1897-1916, doi: 10.1002/(SICI)1097-0207(19991220)46:11;1897::AID-NME758;3.0.CO;2-3.
- [19] G. Stavroulakis, D.G. Giovanis, V. apadopoulos, M. Papadrakakis, "A GPU domain decomposition solution for spectral stochastic finite element method," Solut. Spectr. Stoch. finite Elem. method, 327, (2017) 392-410.
- [20] K. Sepahvand, S. Marburg, "Spectral stochastic finite element method in vibroacoustic analysis of fiber-reinforced composites," Procedia Eng., 199 (2017) 1134-1139, doi: 10.1016/j.proeng.2017.09.241.
- [21] Y. Appalanaidu, A. Roy, S. Gupta, "Stochastic creep damage estimation in pipings with spatial non-Gaussian uncertainties using spectral stochastic finite element method," Procedia Eng., 86 (2014) 677-684, doi: 10.1016/j.proeng.2014.11.069.
- [22] R.G. Ghanem, P.D. Spanos, Stochastic Finite Element Method: Response Statistics. Springer, (1991). doi: 10.1007/978-1-4612-3094-6_4.
- [23] R.G. Ghanem, P.D. Spanos, "Spectral techniques for stochastic finite elements," Arch. Comput. Methods Eng., 4(1) (1997) 63-100, doi: 10.1007/BF02818931.

- [24] S. Zhang, X. Guan, L. Jiang, "Convergence analysis of constraint energy minimizing generalized multiscale finite element method for a linear stochastic parabolic partial differential equation driven by additive noises," J. Comput. Appl. Math., 389 (2021), doi: 10.1016/j.cam.2020.113328.
- [25] J. Schröder, D. Balzani, D. Brands, "Approximation of random microstructures by periodic statistically similar representative volume elements based on lineal-path functions," Arch. Appl. Mech., 81(7) (2011) 975-997, doi: 10.1007/s00419-010-0462-3.
- [26] A. Shaker, W.G. Abdelrahman, M. Tawfik, E. Sadek, "Stochastic finite element analysis of the free vibration of laminated composite plates," Comput. Mech., 41(4) (2008) 493-501, doi: 10.1007/s00466-007-0205-7.
- [27] M. Nadjafi, P. Gholami, "Reliability Study of Notched Composite Laminates Under Uniaxial Loading Based on Continuum Damage Mechanics Approach," Iran. J. Sci. Technol. Trans. Mech. Eng., (2021), doi: 10.1007/s40997-021-00458-w.
- [28] E. Bahmyari, "Stochastic Vibration Analysis of Laminated Composite Plates with Elastically Restrained Edges Using the Non-Intrusive Chaotic Radial Basis Function," Iran. J. Sci. Technol. -Trans. Mech. Eng., (2022), doi: 10.1007/s40997-022-00511-2.
- [29] A. Mouyeaux, C. Carvajal, P. Bressolette, L. Peyras, P. Breul, C. Bacconnet, "Probabilistic stability analysis of an earth dam by Stochastic Finite Element Method based on field data," Comput. Geotech., 101 (2018) 34-47, doi: 10.1016/j.compgeo.2018.04.017.
- [30] M. Kamiński, P. Świta, "Structural stability and reliability of the underground steel tanks with the Stochastic Finite Element Method," Arch. Civ. Mech. Eng., 15(2) (2015) 593-602, doi: 10.1016/j.acme.2014.04.010.
- [31] J. Füssl, G. Kandler, J. Eberhardsteiner, "Application of stochastic finite element approaches to wood-based products," Arch. Appl. Mech., 86(1-2)(2016) 89-110, doi: 10.1007/s00419-015-1112-6.
- [32] M. Lacour, J. Macedo, and N. A. Abrahamson, "Stochastic finite element method for non-linear material models," Comput. Geotech., 125 (2020), doi: 10.1016/j.compgeo.2020.103641.
- [33] C.K. Nowak AS, Reliability of structures. CRC Press, (2013).

- [34] B. Sudret, A. Der Kiureghian, Stochastic Finite Element Methods and Reliability, no. October. (2000).
- [35] C.H. Ma, J. Yang, L. Cheng, L. Ran, "Research on slope reliability analysis using multi-kernel relevance vector machine and advanced first-order second-moment method," Eng. Comput., (2021), doi: 10.1007/s00366-021-01331-9.
- [36] R. Ghanem, G. Saad, A. Doostan, "Efficient solution of stochastic systems: Application to the embankment dam problem," Struct. Saf., 29(3) (2007) 238–251, doi: 10.1016/j.strusafe.2006.07.015.
- [37] P. Zakian, N. Khaji, A. Kaveh, "Graph theoretical methods for efficient stochastic finite element analysis of structures," Comput. Struct., 178 (2017) 29-46, doi: 10.1016/j.compstruc.2016.10.009.
- [38] S.E. Pryse, S. Adhikari, "Neumann enriched polynomial chaos approach for stochastic finite element problems," Probabilistic Eng. Mech., 66 (2021), doi: 10.1016/j.probengmech.2021.103157.
- [39] W.F. Chen, D.J. Han, Plasticity for Structural Engineers. Springer, (1988). doi: 10.1007/978-1-4612-3864-5.

- [40] R. De Borst, M.A. Crisfield, J.J. Remmers, C.V. Verhoosel, Non-Linear Finite Element Analysis of Solids and Structures: Second Edition. JOHN WILEY & SONS, (2012). doi: 10.1002/9781118375938.
- [41] K.J. Bathe, Finite Element Procedures. Prentice-Hall, (2005). [Online]. Available: http://books.google.com/books?id=wKRRAAAA MAAJ&pgis=1%5 Cn-ftp://ftp.demec.ufpr.br/disciplinas/EME748/ Textos/Bathe, K.-J. Finite Element Procedures 1996 Prentice-Hall ISBN 0133014584 1052s.pdf
- [42] J. Huang, D.V. Griffiths, "Return mapping algorithms and stress predictors for failure analysis in geomechanics," J. Eng. Mech., 135(4) (2009) 276-284, doi: 10.1061/(asce)0733-9399(2009)135:4(276).
- [43] S. Im, J. Lee, M. Cho, "Surrogate modeling of elasto-plastic problems via long short-term memory neural networks and proper orthogonal decomposition," Comput. Methods Appl. Mech. Eng., 385 (2021), doi: 10.1016/j.cma.2021.114030.